crystals

MDPI

Article

Interference Induced Enhancement of Magneto-Optical Effect in Pt/TbCo Hetero-Structured Films

Syougo Iemoto [1], Satoshi Sumi [1,*], Pham Van Thach [1,2], Hiroyuki Awano [1] and Masamitsu Hayashi [3,4]

1 Department of Advanced Science and Technology, Toyota Technological Institute, Nagoya 468-8511, Japan; ps3n6cqq@s.okayama-u.ac.jp (S.I.); phamthach@toyota-ti.ac.jp (P.V.T.); awano@toyota-ti.ac.jp (H.A.)
2 Institute of Materials Science, Vietnam Academy of Science and Technology, Hanoi 100803, Vietnam
3 Department of Physics, The University of Tokyo, Bunkyo, Tokyo 113-0033, Japan; mhayashi@qspin.phys.s.u-tokyo.ac.jp
4 National Institute for Materials Science, Tsukuba 305-0047, Japan
* Correspondence: sumi@toyota-ti.ac.jp; Tel.: +81-52-809-1872

Received: 28 August 2018; Accepted: 20 September 2018; Published: 24 September 2018

Abstract: Magnetic films with a heavy metal layer show strong interfacial interaction of spin-orbit. Spin-orbit interaction is one of the key technologies for spintronics. In this paper, we measured magneto-optical Kerr spectra of Pt/TbCo hetero-structure films on a thermally oxidized silicon substrate (0.3 mm); A: Pt (3 nm)/TbCo (6 nm)/Pt (3 nm), B: Si_3N_4 (10 nm)/TbCo (6 nm)/Pt (3 nm), and C: Pt (3 nm)/TbCo (6 nm)/Si_3N_4 (10 nm). Magneto-optical Kerr spectra of each sample were measured with a wavelength range of 300–700 nm, and were compared to the simulated spectra using the effective refractive index method. In the sample A, which has a symmetric structure, the simulated spectra are consistent with the measured ones. On the other hand, in the samples B and C, with an asymmetric structure, there are some differences between the simulated spectra and the measured ones in a lower photon energy region. This may be caused by interfacial effects of the spin-orbit interaction.

Keywords: TbCo; heavy metal; hetero structure; spin-orbit interaction; magnetooptical

1. Introduction

Magnetic films with a heavy metal layer show strong interfacial interaction of spin-orbit, such as the spin Hall effect (SHE) [1–5], the Dzyaloshinskii-Moriya interaction (DMI), and the interfacial Rasba effect [6–8]. These effects change the formation of a magnetic moment at the interface and introduce a spin-state to the interface. Spin-orbit interaction (SOI) is interaction between electron spin and electron orbital angular momentum and related to magneto-optical properties [9–12]. In current-induced domain wall motion (CIDM), these interactions promote a high domain wall (DW) velocity at a lower current density [13–16]. SOI is one of the key technologies for spintronics and its applications. It is important to reveal the SOI in hetero-structure films.

It is known that magneto-optical Kerr effect is a useful method for detecting interfacial information, especially using an optical interference. We reported that large magneto-optical Kerr signals were obtained using ultrathin magnetic films deposited on Si substrates coated with silicon oxide (SiO_2), even for films with magnetic layer of ~1 nm thickness [17]. Multiple reflections in the interface enhanced the magneto-optical effect. And they include interfacial information such as spin-orbit torques, chiral magnetism, and related effects [18–24]. There are many reports about the magneto-optical Kerr effect in a rare earth transition metal (RE-TM) film, with a noble metal layer such as Pt, Pd, etc. [25,26]. However, there are few reports with discussion of the SOI.

In this paper, we measured magneto-optical Kerr spectra of ultrathin Pt/TbCo hetero-structure films with symmetric and asymmetric structures. The measured spectra were compared with the simulated ones using the bulk value of optical constants. Furthermore, the contribution of the SOI to magneto-optical Kerr effect is discussed.

2. Materials and Methods

We prepared three samples on a thermally oxidized silicon (SiO_2,) substrate (0.3 mm); A: Pt (3 nm)/TbCo (6 nm)/Pt(3 nm), B: Si_3N_4 (10 nm)/TbCo (6 nm)/Pt (3 nm), and C: Pt (3 nm)/TbCo (6 nm)/Si_3N_4 (10 nm) Si substrates were sourced from Nakayama Hutech Corporation, Kyoto, Japan. Figure 1 shows structures of these films. The SiO_2 underlayer with thickness of 100 nm was utilized to enhance the Kerr effect thanks to interference [17]. A Si_3N_4 layer was used as a non-heavy metal layer, as well as a protective layer for the TbCo layer. TbCo was deposited by DC magnetron co-sputtering, using Tb and Co targets. TbCo composition was estimated from the deposition rate of each target. Si_3N_4 and Pt were deposited by RF magnetron sputtering using Si_3N_4 and Pt, respectively. Pt, Tb, Co and Si_3N_4 targets were sourced from Chemiston Corporation, Saitama, Japan. All processes were deposited continuously with an Ar pressure of 2 mTorr. Composition of TbCo is $Tb_{40}Co_{60}$ at% with a rare earth-rich feature. Magneto-optical Kerr spectra were measured with a wavelength range of 300–700 nm, using a Xenon light source and a PEM (photo-elastic modulator, model PEM90, HINDS Instruments Inc., Portland, OR, USA). Details are described in ref [27]. Optical indexes were measured by an ellipsometer of JASCO (model M-150, JASCO Corporation, Tokyo, Japan).

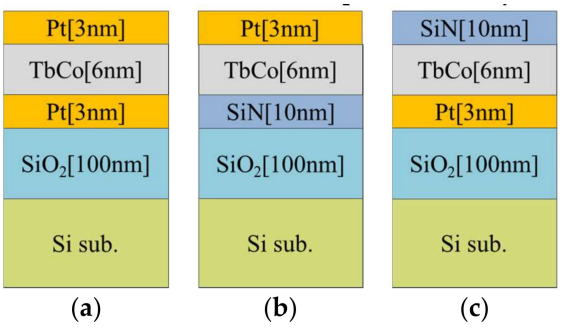

Figure 1. Sample structures. Each sample was deposited on a thermally oxidized silicon (SiO_2 100 nm) substrate (0.3 mm) (**a**) Pt (3 nm)/TbCo (6 nm)/Pt(3 nm), (**b**) Si_3N_4 (10 nm)/TbCo (6 nm) /Pt(3 nm), (**c**) Pt (3 nm)/TbCo (6 nm)/Si_3N_4 (10 nm).

3. Results

Figure 2 shows polar Kerr hysteresis loops of the samples measured with a wavelength of 500 nm. Each sample shows a perpendicular magnetic anisotropy with a different coercivity. Kerr rotation angles were −0.03 degrees for sample A and around 0.11degrees for samples B and C. The polarity of the Kerr rotation angle was opposite between A and B, C, although these samples consisted of a TbCo layer with the same composition.

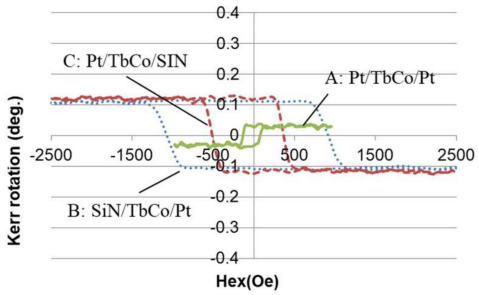

Figure 2. Polar Kerr hysteresis loops of the samples measured with a wavelength of 500nm. A: Pt(3 nm)/TbCo(6 nm)/Pt(3 nm), B: Si_3N_4 (10 nm)/TbCo(6 nm)/Pt(3 nm), C: Pt(3 nm)/TbCo (6 nm) /Si_3N_4 (10 nm).

Figure 3 shows the Kerr spectra of Kerr rotation (θ_K) and ellipticity (η_K) for samples A, B, and C. θ_K and η_K were significantly changed with a wavelength. The θ_K of each sample showed maximum value at a wavelength of around 400 to 500 nm and a sign of each sample changed roughly coinciding with the maximum value of η_K. A peak position of θ_K in the symmetric structure of sample A slightly shifted to shorter wavelengths compared to that in the asymmetric structure of samples B and C. Each η_K in the asymmetric structure samples B and C showed a large angle with longer wavelengths.

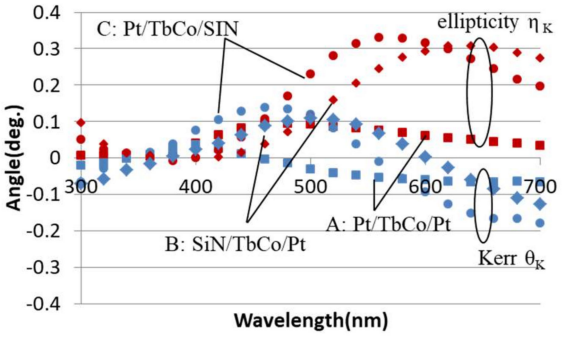

Figure 3. Kerr spectra of Kerr rotation (θ_K) and ellipticity (η_K) for sample A: Pt(3 nm)/TbCo(6 nm)/Pt(3 nm), sample B: Si_3N_4 (10 nm)/TbCo(6 nm)/Pt(3 nm), and sample C: Pt(3 nm)/TbCo (6 nm)/Si_3N_4 (10 nm). Blue and red dots show θ_K and η_K, respectively.

In order to simulate the Kerr spectra, we used the effective refractive index method [28]. Optical constants of the TbCo layer for a right and a left hand circular polarization light were calculated from the measured values of θ_K, η_K, and optical index (n, k) for a 100 nm thick TbCo film in the same method as in Ref. [17]. Figure 4 shows measured and calculated results for a 100 nm thick TbCo film (a) measured Kerr spectrum of θ_K and η_K, (b) measured optical constants (n, k), and (c) calculated optical constants for a right + and a left hand circular − polarization, where real part: N± and imaginary part: K±. The θ_K and η_K of the film monotonously decreased with increasing wavelengths. Optical constants for a right and a left hand circular polarization almost overlapped.

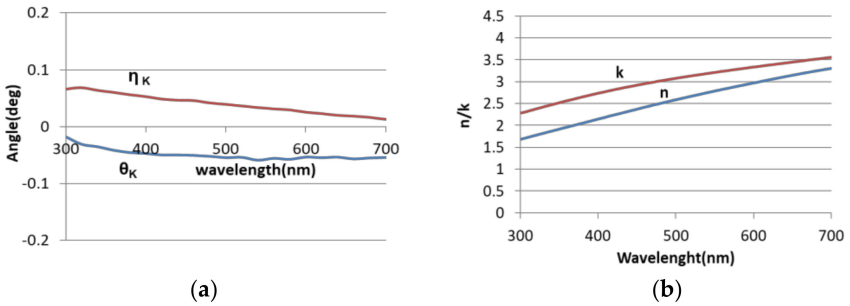

Figure 4. *Cont.*

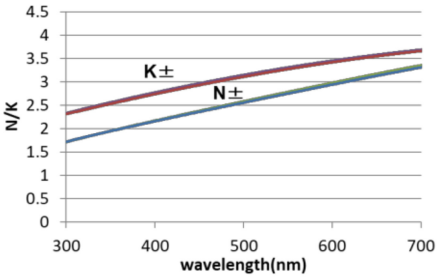

(**c**)

Figure 4. Light wavelength dependence of (**a**) measured Kerr rotation angel (θ_K) and ellipticity (η_K), (**b**) measured optical constants (n, k), and (**c**) optical constants of real part N±, imaginary part K± for a right and a left hand circular polarization calculated from (**a**) and (**b**) for a 100 nm thick TbCo film.

4. Discussion

The Kerr hysteresis loops in Figure 2 and the Kerr spectra in Figure 3 include optical interference in the SiO_2 underlayer and an interfacial effect in the heavy metal of Pt layers. To clarify these contributions, we simulated Kerr spectra using the effective refractive index method as in Refs. [17,28]. In this method, we calculated the refractive index of each layer and effective refractive index from the substrate to i layer, where i is layer number. Repeating this procedure until the top layer, we could obtain an effective refractive index for the whole film. We took optical constants for the TbCo layer in Figure 3, for Pt, Si, SiO_2, and Si_3N_4 in ref [29], which were widely used in the literature.

Figure 5 shows a simulated magneto-optical Kerr spectrum of the sample A deposited on the SiO_2 under layer with thicknesses of 0, 100, 200 nm. The Kerr spectrum θ_K, η_K were enhanced with the SiO_2 underlayer, and were strongly dependent on wavelengths for the films with the SiO_2 underlayer thicknesses of 100 nm and 200 nm. Maximum values of θ_K and η_K in these films were larger than those in a 100 nm thick TbCo film. An optical interference induced significant enhancement of the magneto-optical effect. Moreover, polarity of θ_K in the films with the SiO_2 underlayer with thicknesses of 100 nm and 200 nm changed with wavelengths. At these wavelengths, the η_K showed the maximum value. These results show that the θ_K and η_K have a Kramers-Kronig relation. We could also confirm the relation in Figure 2. At a wavelength of 500 nm, θ_K for the film with a 100 nm thick SiO_2 underlayer shows a small and negative θ_K. One of reasons for the small θ_K and the opposite polarity of the Kerr hysteresis loop in Figure 2 of sample A would be mainly owing to optical interference in the SiO_2 layer.

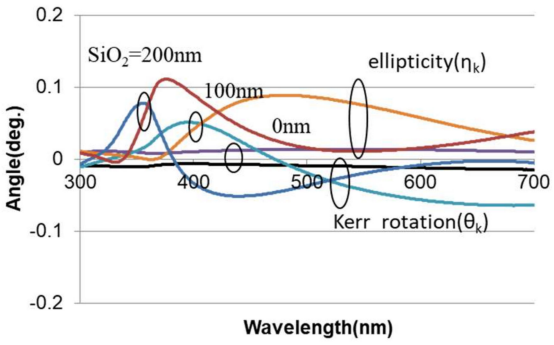

Figure 5. Simulated magneto-optical Kerr spectra of the sample A deposited on the SiO_2 under layer with thicknesses of 0, 100 and 200 nm. Black, blue, and dark blue lines show Kerr rotation θ_K and purple, orange and red lines show ellipticity η_K.

Figure 6 shows the simulated magneto-optical Kerr spectra and the measured ones as a function of photon energy for (a) Pt (3 nm)/TbCo (6 nm)/Pt (3 nm), (b) Si_3N_4 (10 nm)/TbCo (6 nm)/Pt (3 nm), and (c) Pt (3 nm)/TbCo (6 nm)/Si_3N_4 (10 nm). Lines and dots represent the simulated and measured

results, respectively. In sample A with a symmetric structure, the simulated spectra were consistent with the measured ones. On the other hand, in the samples B and C with an asymmetric structure, there were some differences between the simulated and measured results. In a higher energy region, the simulated θ_K and η_K were consistent with the measured ones. In a lower energy region around 2 eV, the simulated θ_K and η_K were smaller than measured ones, especially the η_K. We cannot explain these results by optical interference effects. Reflection lights from the sample include optical and/or magnetooptical properties in each layer. The inverse stack of samples B and C with the asymmetric structures showed almost the same dependencies in the Kerr spectrum. This could have been caused by an enhancement of not optical, but magneto-optical properties. On the other hand, sample A with a symmetric structure showed no enhancement of magneto-optical properties. These results suggest that the spin-orbit interaction at the interface could have been enhanced in the hetero-structure and lead to larger Kerr signals in a lower photon energy region.

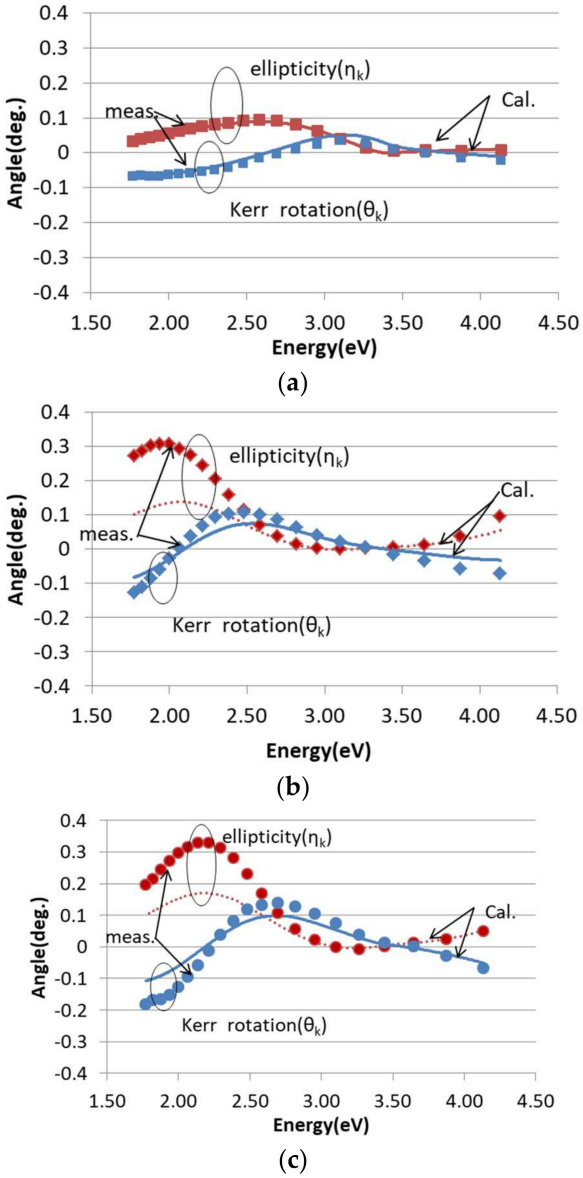

Figure 6. Simulated magneto-optical Kerr spectra of the samples (lines) and measured ones (dots) as a function of photon energy (**a**) Pt (3 nm)/TbCo (6 nm) /Pt(3 nm), (**b**) Si_3N_4 (10 nm)/TbCo (6 nm)/Pt (3 nm) and (**c**) Pt (3 nm)/TbCo (6 nm)/Si_3N_4 (10 nm) Blue dots and lines show Kerr rotation θ_K and red dots and lines show ellipticity η_K.

5. Conclusions

We demonstrated the magneto-optical spectra of Pt/TbCo hetero-structure films. By using a Si substrate with the 100nm of SiO_2 underlayer, we could enhance the magneto-optical Kerr effect to a suitable magnitude. The spectra may include a Kerr effect of the TbCo layer and also an enhanced Kerr effect of Pt/TbCo or TbCo/Pt interface. To clarify these contributions, we simulated Kerr spectra based on the effective refractive index method. In the film with a symmetric structure of Pt/TbCo/Pt, the simulated spectrum was consistent with the measured one. On the other hand, in the films with the asymmetric structures of Pt/TbCo and TbCo/Pt, the simulated spectra were different from the measured ones. In a lower energy region, the measured θ_K and η_K in these films were larger than the simulated ones, especially the η_K. The reason for an enhanced magneto-optical effect may be due to interfacial effects of the spin-orbit interaction.

These results show that Kerr spectra of ultrathin films using an optical interference effect can be utilized to study interface states, including the spin-orbit interaction.

Author Contributions: M.H. and H.A. planned the study. S.I. prepared the films and measured the Kerr spectra. S.I. and S.S. analyzed the results with inputs from P.V.T., H.A. and M.H. All authors have discussed the results and commented on the manuscript.

Funding: This work was partly supported by JSPS Grant-in-Aids for Scientific Research (16H03853, 17H03240), the MEXT-Supported Program Research Foundation at Private University (2014-2019), and Innovation and Spintronics Research Network of Japan.

Conflicts of Interest: The authors declare no conflict of interest.

References

1. Zhang, S. Spin hall effect in the presence of spin diffusion. *Phys. Rev. Lett.* **2000**, *85*, 393–396. [CrossRef] [PubMed]
2. Liu, L.; Pai, C.-F.; Li, Y.; Tseng, H.W.; Ralph, D.C.; Buhrman, R.A. Spin-torque switching with the giant spin hall effect of tantalum. *Science* **2012**, *336*, 555–558. [CrossRef] [PubMed]
3. Bang, D.; Awano, H. Reversal of domain wall motion in perpendicularly magnetized TbFeCo-based wires: Size dependence. *Jpn. J. Appl. Phys.* **2013**, *52*, 123001. [CrossRef]
4. Haney, P.M.; Lee, H.-W.; Lee, K.-J.; Manchon, A.; Stiles, M.D. Current-induced torques and interfacial spin-orbit coupling. *Phys. Rev. B* **2013**, *88*, 214417. [CrossRef]
5. Qiu, X.; Deorani, P.; Narayanapillai, K.; Lee, K.-S.; Lee, K.-J.; Lee, H.-W.; Yang, H. Angular and temperature dependence of current induced spin-orbit effective fields in Ta/CoFeB/MgO nanowires. *Sci. Rep.* **2014**, *4*, 4491. [CrossRef] [PubMed]
6. Bychkov, Y.A.; Rashba, E.I. Properties of a 2D electron gas with lifted spectral degeneracy. *JETP Lett.* **1984**, *39*, 78–81.
7. Dedkov, Y.S.; Fonin, M.; Rüdiger, U.; Laubschat, C. Rashba effect in the Graphene/Ni(111) System. *Phys. Rev. Lett.* **2008**, *100*, 107602. [CrossRef] [PubMed]
8. Caviglia, A.D.; Gabay, M.; Gariglio, S.; Reyren, N.; Cancellieri, C.; Triscone, J.-M. Tunable rashba spin-orbit interaction at oxide interfaces. *Phys. Rev. Lett.* **2010**, *104*, 126803. [CrossRef] [PubMed]
9. Argyres, P.N. Theory of the faraday and kerr effects in ferromagnetics. *Phys. Rev.* **1955**, *97*, 334–345. [CrossRef]
10. Suzuki, Y.; Katayama, T.; Yoshida, S.; Tanaka, K.; Sato, K. New magneto-optical transition in ultrathin Fe(100) films. *Phys. Rev. Lett.* **1992**, *68*, 3355–3358. [CrossRef] [PubMed]
11. Kato, Y.K.; Myers, R.C.; Gossard, A.C.; Awschalom, D.D. Observation of the spin hall effect in semiconductors. *Science* **2004**, *306*, 1910–1913. [CrossRef] [PubMed]
12. Demko, L.; Schober, G.A.H.; Kocsis, V.; Bahramy, M.S.; Murakawa, H.; Lee, J.S.; Kezsmarki, I.; Arita, R.; Nagaosa, N.; Tokura, Y. Enhanced infrared magneto-optical response of the nonmagnetic semiconductor BiTeI driven by bulk rashba splitting. *Phys. Rev. Lett.* **2012**, *109*, 167401. [CrossRef] [PubMed]
13. Bang, D.; Awano, H. High efficiency of the spin-orbit torques induced domain wall motion in asymmetric interfacial multilayered Tb/Co wires. *J. Appl. Phys.* **2015**, *117*, 17D916. [CrossRef]
14. Khvalkovskiy, A.V.; Cros, V.; Apalkov, D.; Nikitin, V.; Krounbi, M.; Zvezdin, K.A.; Anane, A.; Grollier, J.; Fert, A. Matching domain-wall configuration and spin-orbit torques for efficient domain-wall motion. *Phys. Rev. B* **2013**, *87*, 020402(R). [CrossRef]

15. Ryu, K.-S.; Thomas, L.; Yang, S.-H.; Parkin, S. Chiral spin torque at magnetic domain walls. *Nat. Nanotechnol.* **2013**, *8*, 527–533. [CrossRef] [PubMed]
16. Boulle, O.; Rohart, S.; Buda-Prejbeanu, L.D.; Jué, E.; Miron, I.M.; Pizzini, S.; Vogel, J.; Gaudin, G.; Thiaville, A. Domain wall tilting in the presence of the dzyaloshinskii-moriya interaction in Out-of-plane magnetized magnetic nanotracks. *Phys. Rev. Lett.* **2013**, *111*, 217203. [CrossRef] [PubMed]
17. Sumi, S.; Awano, H.; Hayashi, M. Interference induced enhancement of magneto-optical Kerr effect in ultrathin magnetic films. *Sci. Rep.* **2018**, *8*, 776. [CrossRef] [PubMed]
18. Iemoto, S.; Sumi, S.; Awano, H.; Hayashi, M. Magneto-optical properties of Pt/TbCo heterostructure films. In Proceedings of the Abstruct of Intermag 2018 Conference, GW-16, Singapore, 23–27 April 2018; IEEE Magnetics Society: New Jersey, USA.
19. Reigo, P.; Tomita, S.; Murakami, K.; Kodama, T.; Hosoito, N.; Yanagi, H.; Berber, A. Enhanced magneto-optical Kerr effects in Py/Ag/Bi trilayers. *J. Phys. D Appl. Phys.* **2017**, *50*, 19LT01. [CrossRef]
20. Miron, I.M.; Gaudin, G.; Auffret, S.; Rodmacq, B.; Schuhl, A.; Pizzini, S.; Vogel, J.; Gambardella, P. Current-driven spin torque induced by the rashba effect in a ferromagnetic metal layer. *Nat. Mater.* **2010**, *9*, 230–234. [CrossRef] [PubMed]
21. Torrejon, J.; Kim, J.; Sinha, J.; Mitani, S.; Hayashi, M.; Yamanouchi, M.; Ohno, H. Interface control of the magnetic chirality in CoFeB/MgO heterostructures with heavy-metal underlayers. *Nat. Commun.* **2014**, *5*, 4655. [CrossRef] [PubMed]
22. Fan, X.; Celik, H.; Wu, J.; Ni, C.; Lee, K.-J.; Lorenz, V.O.; Xiao, J.Q. Quantifying interface and bulk contributions to spin-orbit torque in magnetic bilayers. *Nat. Commun.* **2014**, *5*, 3042. [CrossRef] [PubMed]
23. Van't Erve, O.M.J.; Hanbicki, A.T.; McCreary, K.M.; Li, C.H.; Jonker, B.T. Optical detection of spin hall effect in metals. *Appl. Phys. Lett.* **2014**, *104*, 172402. [CrossRef]
24. Safeer, C.K.; Jué, E.; Lopez, A.; Buda-Prejbeanu, L.; Auffret, S.; Pizzini, S.; Boulle, O.; Miron, I.M.; Gaudin, G. Spin-orbit torque magnetization switching controlled by geometry. *Nat. Nanotechnol.* **2016**, *11*, 143–146. [CrossRef] [PubMed]
25. Itoh, Y.; Suzuki, T. Magnetic and magneto-optical properties in TbFeCo/(Pt, Pd) multilayers. *J. Appl. Phys.* **2000**, *87*, 6902–6904. [CrossRef]
26. Awano, H.; Niihara, T.; Ojima, M. Magneto-optical and magnetic properties of RE-TM/Pt multilayer films. *J. Magn. Magn. Mater.* **1993**, *126*, 550–552. [CrossRef]
27. Van Drent, W.P.; Suzuki, T. Ultra-violet range magneto-optic study of FCC-Co and Co/Pt multilayers. *J. Magn. Magn. Mater.* **1997**, *175*, 53–62. [CrossRef]
28. Egashira, K.; Yamada, T. Kerr-effect enhancement and improvement of readout characteristics in MnBi film memory. *J. Appl. Phys.* **1974**, *45*, 3643–3648. [CrossRef]
29. Filmetrics Refractive Index Database. Available online: https://www.filmetrics.com/refractive-index-database (accessed on 26 July 2018).